LANGMUIR

pubs.acs.org/Langmuir Article

Using Patterned Self-Assembled Monolayers to Tune Graphene–Substrate Interactions

Maelani Negrito, Meagan B. Elinski, Nathaniel Hawthorne, Mckenzie P. Pedley, Mengwei Han, Matthew Sheldon, Rosa M. Espinosa-Marzal, and James D. Batteas*

Cite This: *Langmuir* 2021, 37, 9996–10005 Read Online

ACCESS | Metrics & More | Article Recommendations | Supporting Information

ABSTRACT: Graphene has unique mechanical, electronic, and optical properties that make it of interest for an array of applications. These properties can be modulated by controlling the architecture of graphene and its interactions with surfaces. Self-assembled monolayers (SAMs) can tailor graphene–surface interactions; however, spatially controlling these interactions remains a challenge. Here, we blend colloidal lithography with varying SAM chemistries to create patterned architectures that modify the properties of graphene based on its chemical interactions with the substrate and to study how these interactions are spatially arrayed. The patterned systems and their resulting structural, nanomechanical, and optical properties have been characterized using atomic force microscopy, Raman and infrared spectroscopies, scattering-type scanning near-field optical microscopy, and X-ray photoelectron spectroscopy.

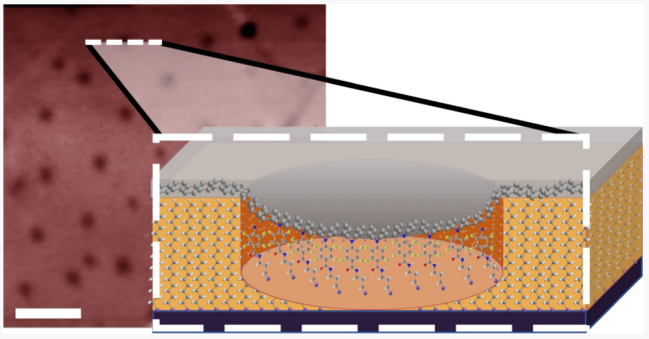

INTRODUCTION

Graphene is an atomically thin 2D honeycomb lattice of sp^2 carbon atoms whose unique electronic and mechanical properties have gained attention for potential use in various electronic, optical, and tribological applications.[1−5] It has a high carrier mobility and excellent thermal conductivity.[3] Graphene has also been shown to exhibit exceptional frictional properties, including yielding superlubricious contacts.[3,5−7] Many studies have shown that these properties of graphene are sensitive to the interactions with the supporting substrate.[1−3,6−10] A work by Lee et al. and Cho et al. showed that out-of-plane deformations of graphene result in an increased frictional force for thinner layers of graphene and that this effect could be controlled through graphene–substrate interactions.[11,12] Stronger graphene–substrate adhesion can greatly reduce the out-of-plane deformation, lowering the friction. Further studies by Spear et al. and Elinski et al. have shown that the frictional behavior of graphene on self-assembled monolayers (SAMs) is sensitive to variations in the functional group (impacting graphene–substrate interaction energy) and SAM chain length (impacting the shear strain).[8,13]

Here, the electronic properties of graphene have also been shown to be influenced by substrate interactions via charge doping effects.[14−16] Clean, hydrophilic silica, for example, exhibits high electron–hole charge amplitude fluctuations, which result in regions that are highly p-doped.[15] These charge fluctuations, also known as charge puddles, scatter charge carriers in graphene,[15] which can not only influence carrier mobility in graphene[17] but, via charge donation, can also impact the reactivity of exfoliated graphene.[15] These effects can be modulated through the application of SAMs such as octadecyltrichlorosilane (OTS), which acts to decrease the effects of these charge fluctuations by increasing the distance between graphene and the substrate, screening such effects. Beyond noncovalent interactions, covalent functionalization of graphene has attracted attention as an approach to opening the band gap of graphene, tuning its conductivity.[18,19] Band gap opening has also been carried out via patterning of graphene, by oxidative removal of graphene in spatially arrayed patterns, and introducing scattering defects into the graphene lattice.[20−22]

In the work described here, we seek to combine the effects of patterning with substrate chemical modification to elucidate the interplay of these on the structural, mechanical, and optoelectronic properties of graphene deposited on these modified surfaces. To accomplish this, a background SAM of OTS is templated using colloidal lithography onto oxidized silicon wafers to create nanoscale pores of ca. 2 nm in depth in a hexagonal arrangement with the spacing dictated by the

Received: April 26, 2021
Revised: July 20, 2021
Published: August 10, 2021

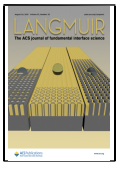

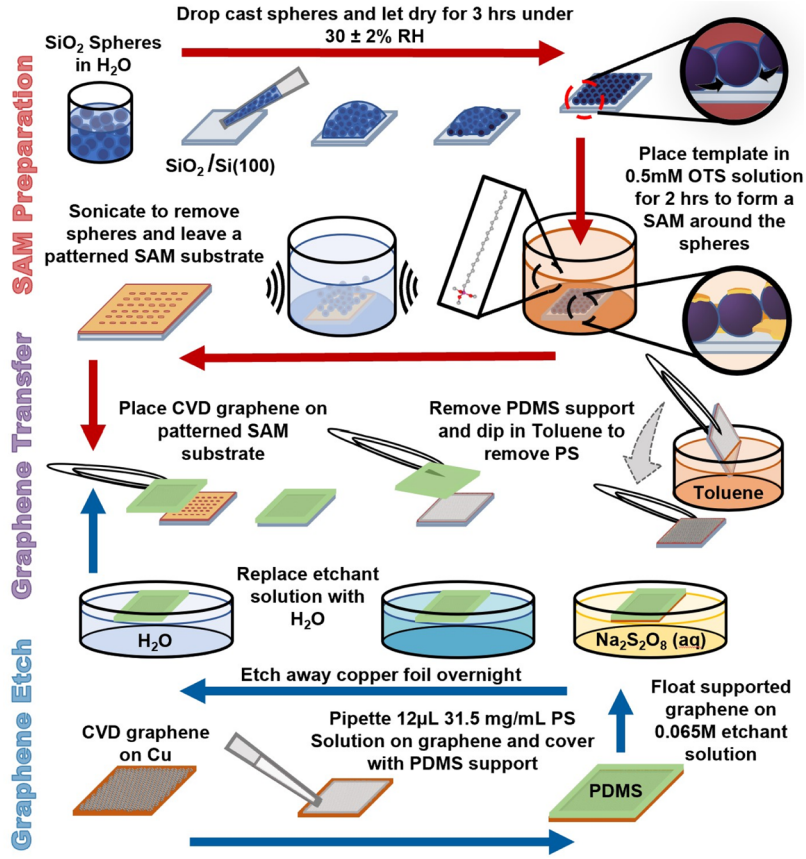

Figure 1. Schematic of the template self-assembly, chemical vapour deposition (CVD) graphene preparation, and subsequent transfer to a patterned SAM substrate.

dimensions of the colloid used.[23] The pores are then left empty or back-filled with either a different silane—decyltrichlorosilane (C10) or a perfluorophenylazide *N*-(3-trimethoxysilylpropyl)-4-azido-2,3,5,6-tetrafluorobenzamide (PFPA) to make mixed SAMs onto which graphene is deposited to spatially tailor the chemical interactions between them. As the graphene is seen to conform to the patterned surface, the comparison between empty and C10- or PFPA-filled pores allows us to examine how local structural distortion of the graphene interplays with spatial chemical interactions, including the spatial disruption of the double bond network of the graphene via reaction of the graphene with PFPA, which can be covalently linked to graphene via a ring insertion of the nitrene group.[18,24−27] The fabrication of such a composite interface has a number of benefits, including providing an internal reference to compare changes in the mechanical and optoelectronic properties of graphene in the presence of these modified surfaces, as these properties are well studied for graphene−OTS surfaces. Each step of producing the structure was characterized with atomic force microscopy (AFM) and attenuated total reflection Fourier transform infrared (ATR−FTIR) spectroscopy. Additionally, after transferring graphene to the samples, Raman microspectroscopy, X-ray photoelectron spectroscopy (XPS), and scattering-type scanning near-field optical microscopy (s-SNOM) were also used to characterize the graphene−pore samples. Thus, the structures characterized here can serve as a versatile platform to study many of the unique properties of graphene such as the frictional response and mechanical stability, van der Waals screening, and optical properties with a built-in reference and easily modified periodicity and pore dimensions.

EXPERIMENTAL METHODS

Substrate Preparation. The base substrates used in all cases described in this work are single-side polished Si(100) wafers (Virginia Semiconductor) with 90 nm of thermal oxide grown on them. To prepare these, the wafers were score cut and cleaned by soaking in a base piranha solution of a 4:1:1 (v/v/v) ratio of nanopure water (18.2 MΩ·cm, Barnstead), concentrated NH_4OH, and H_2O_2 (30% wt) at 85 °C for 20 min before being rinsed thoroughly with nanopure water and then with 200 proof ethanol and dried with streaming N_2. The cleaned wafers were then thermally oxidized in a kiln at 1050 °C for 30 min to produce the thermal oxide film on the Si(100) surface. Afterward, the SiO_2/Si(100) surfaces were again cleaned with a base piranha solution at 85 °C for 20 min and rinsed and dried as before.

Patterning of Silane-Based SAMs Using Colloidal Lithography. To prepare patterns of OTS on the surfaces, the clean and oxidized Si substrates described above were patterned using colloidal sphere lithography. To evaluate the effects of pattern periodicity, three sizes of SiO_2 spheres [0.2 μm, 0.5 μm (NIST), and 1.8 μm diameter (NANOCYM)] were centrifuged at 3400 rpm for 5 min, the supernatant was removed, and the spheres were covered and stored overnight to dry. The SiO_2 spheres were then suspended in nanopure water to achieve a ca. 4% (w/v) solution (Figure 1). Immediately after preparing the oxidized substrates described above, 10 μL of the 4% w/v SiO_2 sphere solution was drop-cast onto the wafer. The drop-cast wafers were then placed in a nitrogen tent (Captair Pyramid, Erlab) with a relative humidity, RH, of 30 ± 2%, controlled by bubbling nitrogen through water into the tent and were left to dry for 3 h. This produced a close-packed hexagonal pattern upon drying with feature spacing equivalent to the particle diameter.

https://doi.org/10.1021/acs.langmuir.1c01136
Langmuir 2021, 37, 9996−10005

After drying, the sphere-templated wafers were placed in a dry N_2 environment (<0.1% RH) where they were immersed in a 0.5 mM solution of *n*-OTS (Gelest) in toluene and allowed to react for 2 h to form a templated SAM. To remove the SiO_2 spheres and any physisorbed OTS, the wafers were sonicated for 45 min in a series of solvents (once in fresh toluene and twice in fresh ethanol), rinsing the wafers with ethanol in between sonication cycles. After the final ethanol sonication, the wafers were rinsed with water and then ethanol and dried with streaming N_2.

Back-Filling Pores with C10 or PFPA. To create a mixed monolayer, the templated OTS SAMs were back-filled with either C10 or PFPA. For the C10-filled pores, the OTS-patterned wafer was soaked in a 0.5 mM decyltrichlorosilane (C10, Gelest) in toluene solution and allowed to react for 2 h. The wafers were sonicated for 1 h in subsequent solvents (once in fresh toluene and twice in fresh ethanol), rinsing the wafers with ethanol in between sonication cycles. After the final ethanol sonication, the wafers were rinsed with water and then ethanol and dried with streaming N_2. For the PFPA-filled pores, a solution of 0.1 mM PFPA (>90%, Toronto Research Chemicals, Inc.) in toluene was prepared and the OTS-patterned wafer was allowed to react in the dark for 4 h (Figure 2A). After reacting, the wafer was cleaned by rinsing with toluene before being sonicated in fresh toluene for 10 min at room temperature (~21.3 °C), rinsed with nanopure water and then ethanol, sonicated in ethanol for 10 min, and subsequently being rinsed with nanopure water and then ethanol and dried with streaming N_2.

Reference PFPA Monolayer Preparation. To provide an additional control sample, an oxidized Si(100) substrate with a full PFPA monolayer was prepared using the same procedure as described in back-filling the pores where a solution of 1 mM PFPA (>90%, Toronto Research Chemicals, Inc.) in toluene was prepared and the base-piranha cleaned SiO_2/Si(100) wafer was allowed to react in the dark for 4 h. After reacting, the wafer was cleaned by rinsing with toluene before being sonicated in fresh toluene for 10 min at room temperature (21.3 °C), rinsed with nanopure water and then ethanol, sonicated in ethanol for 10 min, and subsequently being rinsed with nanopure water and then ethanol and dried with streaming N_2.

Graphene Transfer and Reaction with Azide. Following SAM preparation, graphene was transferred (Figures 1 and 2A) onto the desired substrates (a PFPA monolayer, empty pores formed by the OTS matrix, PFPA-filled pores, or C10-filled pores) via a dry-transfer method.[28] A section of CVD graphene (LG) on copper was coated with a 31.5 mg/mL solution of polystyrene (PS, M_w 13,000, Sigma-Aldrich) in toluene as a self-releasing layer (SRL) and heated at 80 °C for 5 min to remove residual solvent. The SRL is used to facilitate the removal of the polydimethylsiloxane (PDMS) stamp after transferring the graphene.

A PDMS (Dow Inc.) stamp (~0.5 mm thickness) was then placed on top of the PS-coated graphene as a support. The graphene on the copper stack was then placed on top of a 0.065 M solution of sodium peroxydisulfate (Alpha Aesar) for at least 6 h to etch away the underlying copper. Once the copper was removed, the etchant solution was carefully displaced by flowing clean Millipore water. Afterward, the graphene−PS−PDMS was removed from the water surface and placed onto the patterned SAM substrate using tweezers and left in a vacuum desiccator to dry. The sample was then heated to 100 °C for 5 min to reach the glass transition temperature of the PS SRL layer, and the PDMS was removed using tweezers. The graphene-covered sample was then dipped in fresh toluene to remove residual PS from the surface. To further drive covalent bonding between the graphene and PFPA (either on the patterned surfaces or the monolayer), samples were heated at 140 °C for 40 min under ambient conditions (Figure 2B).[18] As described in the literature, upon heating, one of the N−N double bonds breaks allowing for the loss of an N_2 group, thereby leaving a nitrene end group, which then undergoes a [2 + 1] cycloaddition reaction with the graphene lattice.[18,25,26]

Raman Microspectroscopy. Characterization of the graphene by Raman spectroscopy was conducted using a WiTec Alpha 300RA (Germany) confocal microscope with an ultrahigh throughput

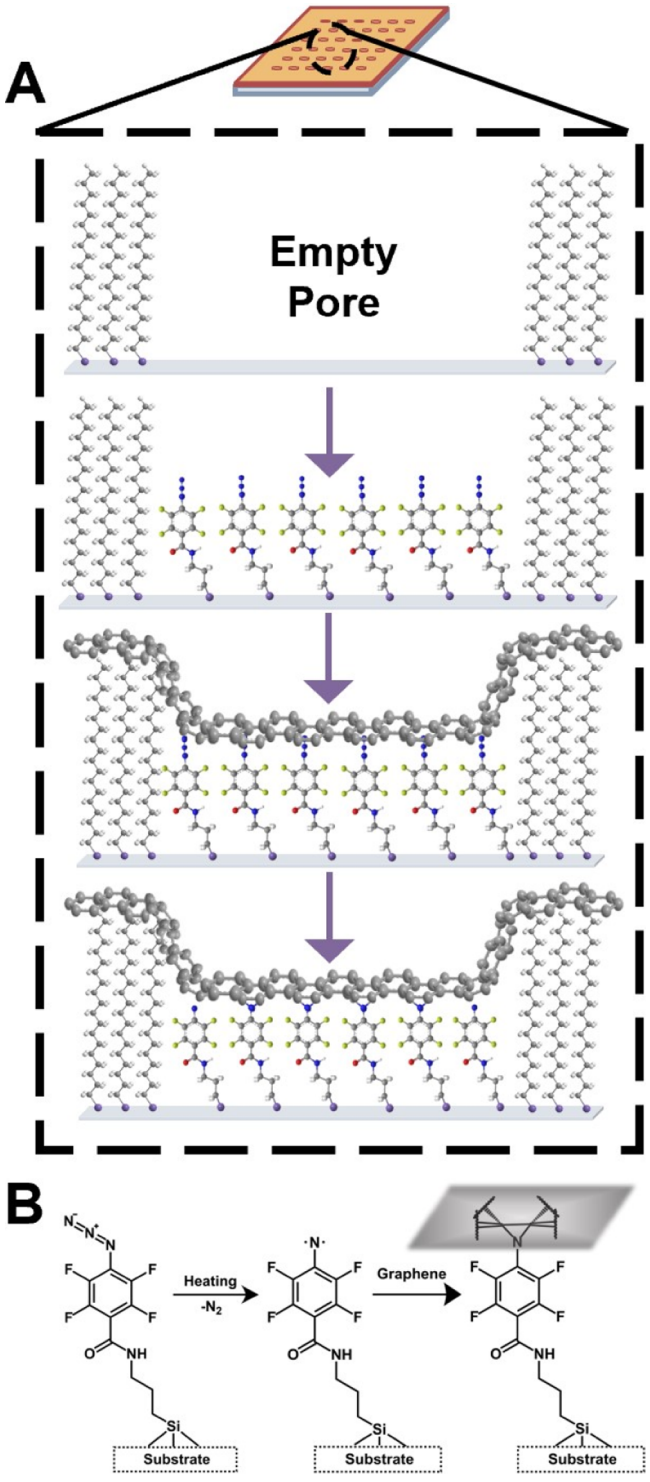

Figure 2. Schematic of back-filling pores with PFPA molecules and subsequent reaction with graphene. (A) Empty pores in the OTS monolayer are back-filled with PFPA molecules before transferring CVD graphene onto the patterned SAM. The graphene−SAM architecture is then heated at 140 °C for 40 min to drive the reaction between the azide group of the PFPA molecule and two adjacent carbon atoms in the graphene lattice. (B) Reaction mechanism of the PFPA azide group with graphene.

spectrometer (UHTS 300) using a 600 blaze grating and an Andor DV401A CCD detector. A 532 nm Nd:YAG laser with a power of <1.5 mW was focused to a spot size of ~360 nm with a Zeiss high numerical aperture objective (100×, 0.9 NA). The graphene layer

https://doi.org/10.1021/acs.langmuir.1c01136
Langmuir 2021, 37, 9996−10005

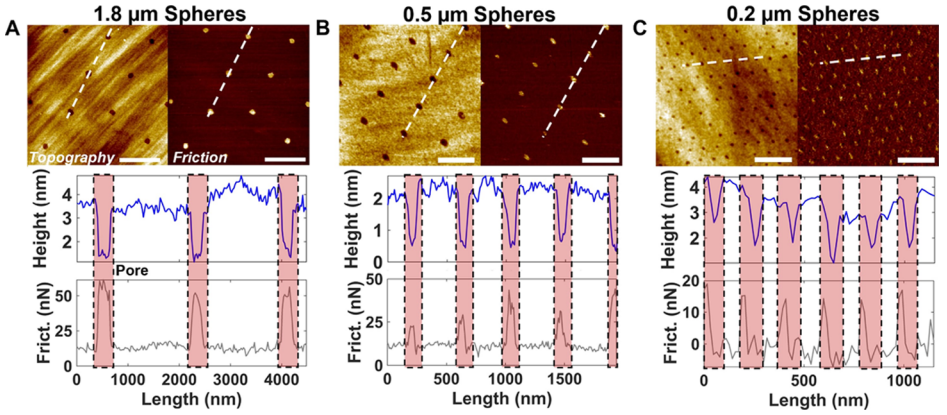

Figure 3. AFM topography and friction images and cross sections for pores in OTS monolayers using three different template sphere diameters. Topography and friction images with corresponding cross sections of empty pores using a template of (A) 1.8 μm spheres, (B) 0.5 μm spheres, and (C) 0.2 μm spheres. For all images, cross-sectional locations are indicated by white dashed lines and pores are indicated in cross sections by pink boxes. Scale bars are (A) 2, (B) 0.5, and (C) 0.5 μm.

Table 1. Pore Dimensions before and after Modification

		no graphene		with graphene	
template sphere diameter (μm)	pore type	average pore fwhm (nm)	average pore depth (nm)	average pore fwhm (nm)	average pore depth (nm)
1.8	empty	190.4 ± 30.5	2.0 ± 0.2	182.4 ± 32.0	1.9 ± 0.3
	PFPA	228.3 ± 49.0	1.3 ± 0.2	214.6 ± 47.2	1.3 ± 0.2
	C10	175.5 ± 41.5	1.2 ± 0.2	169.8 ± 30.9	1.3 ± 0.2
0.5	empty	117.6 ± 21.4	1.9 ± 0.4	87.4 ± 27.8	1.7 ± 0.5
	PFPA	114.4 ± 22.2	1.1 ± 0.3	75.3 ± 18.0	1.1 ± 0.3
	C10	110.3 ± 17.2	1.1 ± 0.3	76.2 ± 16.2	1.1 ± 0.2
0.2	empty	64.4 ± 20.2	1.9 ± 0.4	58.4 ± 12.2	1.8 ± 0.2
	PFPA	52.9 ± 16.7	1.1 ± 0.3	45.9 ± 12.7	1.1 ± 0.3
	C10	50.3 ± 14.3	0.9 ± 0.3	49.5 ± 9.0	0.9 ± 0.3

thickness was confirmed by mapping the 2D/G ratio, where a 2D/G ratio of >2.0 is indicative of a single layer.[29−35]

X-ray Photoelectron Spectroscopy. XPS was performed on a bare and a graphene-covered PFPA monolayer to investigate the chemical reaction with graphene. Here, an Omicron DAR 400 dual Mg/Al X-ray source was used, with a 128-channel microchannel plate Argus detector, with a base pressure in the high 10^{-10} mbar range. High-resolution spectra were taken using the Mg (1253.6 eV) source at 10 kV and 4 mA, for a power of 40 W. Spectra shown were taken with a 40 eV pass energy, 0.05 eV step size, and a 0.3 s dwell time. Due to the rapid rate at which the PFPA monolayer degrades under exposure to X-ray irradiation, a single spectrum was taken for each of the samples before and after heating, and all spectra were calibrated by setting the preheat amide N (1s) peak to 400.5 eV,[36] offsetting the postheat spectrum for each type by that same amount, instead of running additional reference spectra in another energy range. The full width at half-max (fwhm) for all N (1s) peaks in a spectrum was constrained to be the same.

FTIR Spectroscopy. ATR−FTIR spectroscopy was used to characterize the SAM-functionalized silica wafers. Spectra were collected with a Thermo Nicolet 6700 FTIR with a germanium ATR crystal and a liquid nitrogen-cooled MCT (HgCdTe) detector, averaging 2000 scans with a 1 cm^{-1} resolution. The reference PFPA monolayer was prepared to verify the reaction of graphene to PFPA. Spectra were taken of the same oxidized Si wafer before and after the addition of a uniform PFPA monolayer, after exfoliating graphene, and after thermally reacting the graphene with the PFPA.

Atomic Force Microscopy. Simultaneous topography and friction images were collected with an Agilent 5500 in air at a nominal applied load of 5 nN. Data analysis was performed using the software program scanning probe image processing (SPIP). Silicon tips (μMasch) with nominal spring constants of ca. 0.3 N/m and radii of ca. 20 nm were used in contact mode. The spring constants were determined in situ via the Sader method,[37] and the radii were determined experimentally using the blind tip reconstruction feature of SPIP.

Scattering-Type Scanning Near-Field Optical Microscopy. s-SNOM was employed to assess the impact of nanotexturing and periodic covalent binding of graphene on the surface plasmon polariton (SPP) of the graphene sheet. Data were collected using a nanoIR2-s System (Anasys Instruments) in an ambient environment (23 °C and 50% RH). AFM tapping mode images were simultaneously collected with near-field (NF) amplitude images (as the absolute value of the NF signal). Platinum-coated silicon AFM tips were used with a nominal tip radius of ∼50 nm and resonance frequency of ∼270 kHz. A CO_2 laser (λ: 10.5 μm, or 952 cm^{-1}) was used as the NF source, focused through a numerical aperture of 0.3. Changes in the amplitude of the scattered NF signal were imaged at the third harmonic of the resonance frequency using a double demodulation process to separate the background signal from the scattered NF signal and imaged in an interleave mode to subtract the DC signal offset from the far field. A liquid nitrogen-cooled MCT detector was used. Data analysis was performed in Analysis Studio v3.12.

RESULTS AND DISCUSSION

Patterning of Empty, C10-Filled, and PFPA-Filled Nanopores on the Oxidized Si(100) Surface. The first step in our sample preparations was to create patterned arrays of empty pores in an OTS SAM. Here, as described in the methods section, colloidal lithography was employed to create nanostructured surfaces using silica nanoparticles of 1.8, 0.5, and 0.2 μm in diameter to control the pattern pitch. Following assembly of these spheres into hexagonal patterns on the

https://doi.org/10.1021/acs.langmuir.1c01136
Langmuir 2021, 37, 9996−10005

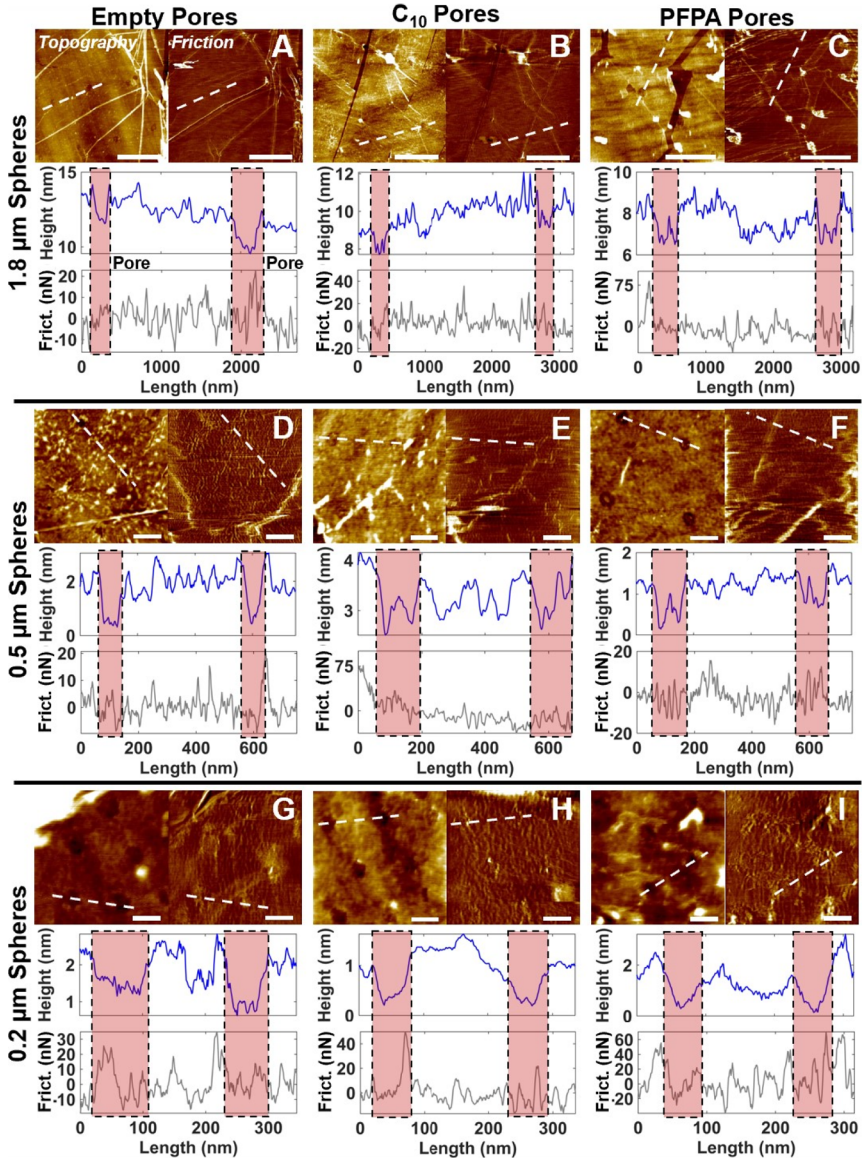

Figure 4. AFM topography and friction images with corresponding cross sections for graphene transferred onto pores created using a template of 1.8 (A–C), 0.5 (D–F), and 0.2 μm (G–I) spheres, showing topographic and friction images with corresponding cross sections of empty pores (left column) and C10-filled (center column) and PFPA-filled pores (right column). For all images, cross-section locations are indicated by white dashed lines, where pore positions are highlighted in pink. The scale bars are 2 μm (A–C), 200 nm (D–F), and 100 nm (G–I).

surface,[23,38] OTS SAMs formed in all of the exposed surfaces between the silica particles, which, when the silica particles are removed leaves open pores on the surface of ca. 2 nm in depth with periodic spacing defined by the particle diameter and assembly symmetry.

The morphology of the patterned OTS on silica substrates was examined by contact mode AFM to determine the feature sizes (Figure 3). Silica microspheres of three diameters, 1.8, 0.5, and 0.2 μm, were used as templates to vary pore diameter and pitch. As has been seen by others using colloidal lithography for patterning of SAMs,[23] the pitch was determined by the silica sphere diameter and with the pore depth determined by the thickness of the OTS monolayer of ca. 2 nm[39−42] with pore diameters ranging from ca. 180 nm in diameter for the largest spheres down to ca. 50 nm in diameter for the smallest spheres (Table 1). Histograms of the pore dimensions with and without the deposited graphene are given in the Supporting Information Figures S1−S6.

To examine the effects of substrate interactions on graphene deposited on these patterned monolayers, the empty pore structures were subsequently filled with decyltrichlorosilane (C10) or PFPA to examine both the impact of charge screening and spatial covalent bonding on the physical properties of single-layer graphene deposited on these films. Upon back-filling the empty pores with C10 or PFPA, the average pore depth decreases to ca. 1 nm, consistent with the physical height differences between OTS and either C10 or PFPA, while, as expected, there was no noted difference in pore diameter (Table 1) within error bars.

Deposition of Graphene on the Patterned Surfaces. To examine the effects of the substrate patterning on the physical properties of graphene, CVD graphene was transferred onto the patterned substrates and subsequently characterized by AFM, FTIR, XPS, and Raman microspectroscopy. Structurally, on each substrate, graphene was seen to strongly adhere to the surface and follow the contours of the nanopore

https://doi.org/10.1021/acs.langmuir.1c01136
Langmuir 2021, 37, 9996−10005

features (Figure 4). This is consistent with our prior studies, showing high adhesion between graphene and OTS SAMs.[8,13] From these measurements, the graphene is observed to be conformed to the surface features as evidenced by the pore depth (Table 1) coinciding with the expected depth. In contrast to uncovered pores, the friction of the graphene sheet was seen to remain nominally consistent across all of the surface regardless of the pore size or underlying surface chemistry within the pores, as the friction response is dominated by the overlying graphene sheet (Figure 4). As a result, the pores can be seen in the topography image but not the corresponding friction image. In contrast, if the graphene did not adhere to the contours of the features, it is expected that the friction would increase due to the graphene puckering up under the AFM tip as it slides over the surface.[11]

Unlike the methyl-terminated regions of the SAMs, the graphene may be further modified by covalently bonding it to the underlying PFPA by heating to 140 °C.[18] As such, we also examined the effects of temperature on these structures. As mentioned above, in each case, the graphene was still conformed to the underlying features, but the overall friction was observed to decrease by ∼50% as compared to the nonheated case. This can be attributed to the change in strain in the graphene lattice upon heating resulting from the negative thermal expansion coefficient of graphene.[35,43,44] There was compressive strain in the graphene sheet from the transfer process.[45] Upon heating, the difference in the thermal expansion of graphene and the underlying substrate typically results in increased tensile strain, where the overall friction decreases with the increasing tensile strain.[35,46,47] In this case, the compressive strain is reduced, thereby lowering the friction.

In addition to the noted overall decrease in friction for all three pore types following heating, the PFPA-filled pores exhibited a further 30−50% decrease in friction localized to the PFPA-filled pores (Figure 5). We attribute this to the azide

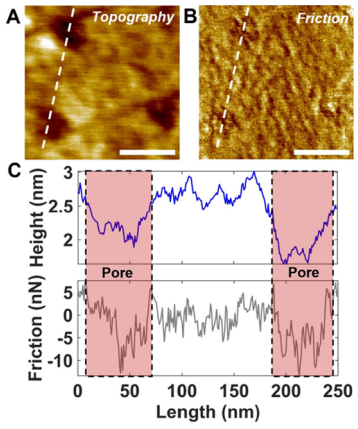

Figure 5. AFM topography (A) and friction (B) images with corresponding cross sections (C) for graphene reacted to 0.2 μm PFPA-filled pores. For both images, cross-section locations are indicated by white dashed lines and scale bars are 0.1 μm.

group of the PFPA molecules reacting to the graphene sheet, further pinning the structures, whereby the reacted PFPA molecules act to tether the graphene to the underlying surface thus inhibiting the out-of-plane deformation that dominates the friction measurement in an AFM scan.[9,11] The additional decrease in friction due to reaction with PFPA was further confirmed by measuring graphene exfoliated onto a monolayer of PFPA before and after reaction (see Supporting Information Figure S7).

To extend upon the topological characterization, Raman microspectroscopy was used to determine layer thickness of the graphene flakes and to characterize the samples before and after heating at 140 °C for 40 min (Figures 6 and 7). The ratio of the 2D/G peak intensities is reported in blue for each spectrum in Figure 6, where a ratio >2.00 indicates single-layer graphene.[29−31,33,35,43] Despite disruption of the graphene lattice being covalently linked to the PFPA pores, the appearance of a D peak was not observed for our samples. While this is not surprising, as the pore diameter (∼200 nm) is much smaller than the laser spot size (∼360 nm, diffraction limited) of our Raman measurements. The D peak also did not appear in the PFPA reference sample, where graphene was exfoliated onto a PFPA ML.

This is consistent with previous studies,[18,24] with the lack of an appearance of a D peak with functionalization, suggesting that the sp^2 network is not disrupted.[18,25,26,48−50] Only defects that scatter electrons between the valleys of the electronic dispersion of graphene can contribute to the D-peak.[30,48−50] As the nitrene [2 + 1] cycloaddition largely preserves the linear dispersion near the Dirac point, the sp^2 network is also maintained[25,26] and, thus, does not scatter electrons.

While it is difficult to fully separate the effects of strain and doping on the Raman spectrum, as with determining the layer number, the ratio of the 2D/G position can still provide qualitative information.[31,45] Following the work by Lee et al.,[31] the shift in the peak position from the intrinsic peak positions without strain or doping (values from ref 31) can be used to indicate whether the shift in peak position is influenced more by strain or doping. The ratio of the 2D peak position shift to the G peak position shift is used to discern the cause of the shift in peak positions, where a large ratio ($\gtrsim$2.00) indicates that the shift is primarily a result of strain,[31,32,45,51] where an upshift in the G peak position is indicative of compressive strain and a downshift in the G peak position is indicative of tensile strain.[45,51] Smaller ratios indicate the shift in peak positions are influenced more from doping.[31,32,45,51] These ratios are reported in red for each spectrum in Figure 6. The large ($\gtrsim$2.00) ratios in this work indicate that the shift in the G peak position is a result of strain in the graphene lattice where the upshift in the G peak position, indicated by the sign in parenthesis next to the G peak label, signifies that the observed strain is compressive, albeit reduced after heating. This reduction in compressive strain supports our observation of an overall decrease in the friction of graphene across all pore types after heating at 140 °C.

ATR−FTIR spectroscopy was also performed on the PFPA monolayer control samples (Figure S8) to confirm reactivity. The azide stretch at ∼2124 cm^{-1} is clearly present for the PFPA monolayer. Upon graphene exfoliation, the peak intensity decreases slightly and subsequently disappears after heating at 140 °C for 40 min (Figure S8B). As a reference, another PFPA monolayer control—without graphene—was examined. The PFPA monolayer was heated for 40 min at 140 °C and 2 min at 80 °C to mimic the conditions of the graphene−PFPA reaction procedure and graphene exfoliation procedure, respectively. As shown in Figure S8A, the azide peak also disappears entirely after being heated at 140 °C for 40 min in an oven but remains after being heated at 80 °C for 2 min, thus verifying the reaction does not occur during the graphene exfoliation process.

https://doi.org/10.1021/acs.langmuir.1c01136
Langmuir 2021, 37, 9996−10005

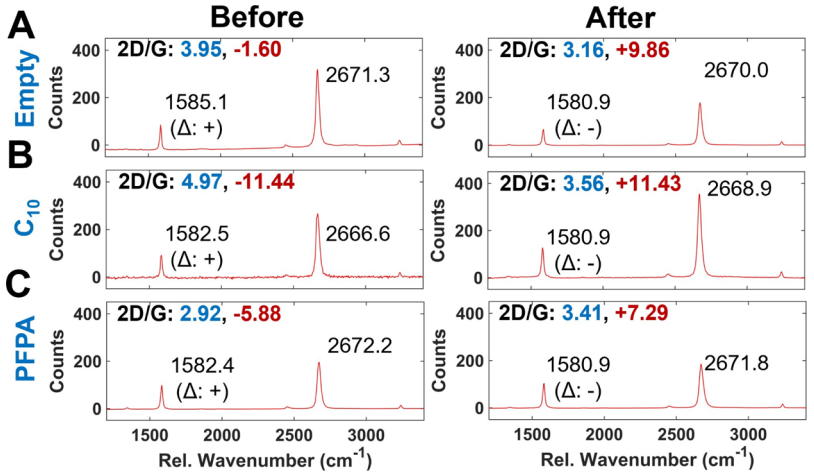

Figure 6. Representative Raman spectra of graphene over the various 1.8 μm pore samples before and after heating. (A) 1.8 μm empty pores, (B) 1.8 μm C10-filled pores, and (C) 1.8 μm PFPA-filled pores. For all spectra, the 2D (~2670 cm^{-1}) and G (~1583 cm^{-1}) peak positions are labeled in black, the 2D/G peak intensity ratios are labeled in blue, and the ratio of the shift (Δ) in 2D/G peak positions are labeled in red. The peak shifts are calculated using the intrinsic peak positions (G: 1581.6 cm^{-1} and 2D: 2676.9 cm^{-1}) from the study by Lee et al. (ref 31), where large (>2.00) 2D/G peak shift ratios indicate that the shift in peak position is dominated by strain. When the shift in peak positions is dominated by strain, the direction of the G peak shift, indicated in parenthesis in each spectrum, denotes the type of strain. An upshift (Δ: +) signifies compressive strain, whereas a downshift (Δ: −) signifies tensile strain.

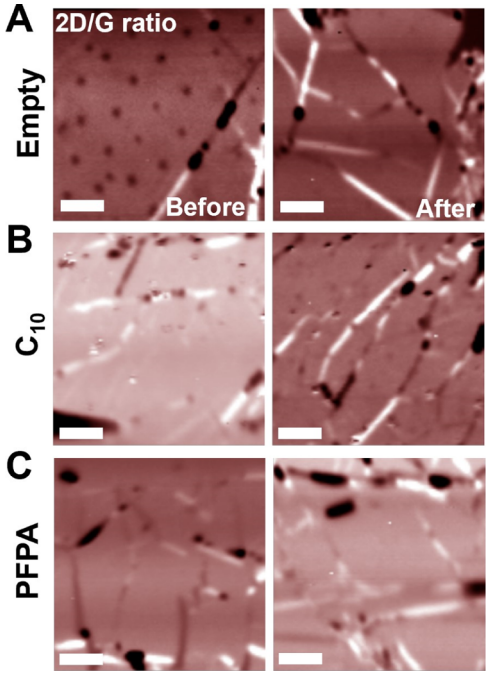

Figure 7. Raman maps from graphene over a larger pore system (the 1.8 μm microsphere template) for empty pores (A), C10 pores (B), and PFPA pores (C) before and after heating at 140 °C. Scale bars are 2 μm.

While the FTIR data confirm the removal of the azide group as a result of heating, the disappearance of a peak cannot unambiguously prove that a reaction takes place between the remaining nitrene and the graphene, the N (1s) peaks using XPS were compared before versus after reaction to confirm the reaction.[18,24,27,36] Here, X-ray photoelectron spectra were taken of a bare PFPA monolayer and a graphene-covered PFPA monolayer before and after heating (Figure S9). The peak information for each spectrum is displayed in Table S1. From Figure S9A,C and Table S1, the spectra before heating is similar for bare and graphene-covered PFPA, with the total signal for the covered PFPA slightly less due to partial screening by the graphene.

In both cases, the spectra agree with the literature, with the peak representing the outer two nitrogen in the azide at 402 eV about double that of the center nitrogen, at 405 eV.[24,36] After heating, the bare PFPA only has one broad peak at 400.05 eV (Figure S9B and Table S1), likely due to a combination of the amide peak and nitrogen products produced from degradation of the azide. The graphene-covered PFPA monolayer can be fit with two peaks after heating, at 400.55 and 402.42 eV (Figure S9D and Table S1), indicating some of the azide remains, as it formed the cycloaddition product with graphene. The ratio between these two peak areas of 1.7 is similar to the reported literature value of 1.9.[42] The differences in the post-heated XPS spectra for bare and graphene-covered PFPA, along with the IR spectra shown in Figure S8, are strong evidence that the graphene is chemically bonded to the azide.

Influence of the Nanopore Patterns on the Electronic Properties of Graphene. In addition to its mechanical properties, graphene's electronic properties are also sensitive to the chemistry of the substrate on which it is deposited. The substrate has been shown to have a doping effect on graphene, where silica, for example, typically results in p-type doping where several studies have illustrated the dependence of graphene's Raman spectra on both strain and charge density.[15,30]

To examine such effects here, Raman microspectroscopy maps were taken of the larger pore system using the 1.8 μm microsphere template. The ratio of the characteristic Raman peaks, 2D and G, for all three pore types (empty, C10, and PFPA) before and after heating is shown in Figure 7 with representative spectra from the maps shown in Figure 6. While Raman was performed on all samples to confirm the graphene layer thickness, the pores were only visible in the Raman maps for the larger pore size. This is most likely due to smaller diameters of the pores being below the spatial resolution of the instrument due to the diffraction limit. It is important to note that while pores could only be seen in the Raman maps with

https://doi.org/10.1021/acs.langmuir.1c01136
Langmuir 2021, 37, 9996−10005

the large pores, they were not discernible in every scan. However, this shows that the graphene has sufficient interaction with the substrate local to the pores to observe clear spatial effects of charge doping and strain on the 2D/G peak ratios. Also, after heating, as denoted in the topographic measurements, these differences in the 2D/G intensities are no longer observed, which would be consistent with the graphene becoming tauter, thereby reducing its interaction with the silica substrate.

Further impacts of the patterned pore structures on the optoelectronic properties of graphene could be observed when evaluating NF scattering effects in the infrared. Here, s-polarized SNOM imaging was employed to examine any changes in the propagating SPP of graphene over the patterned nanopores by comparing pore samples with and without PFPA both before and after heating. Propagating SPP waves in graphene are the coupled excitations of photons and charge carriers[52] and depend on substrate-induced doping and the local carrier density.[52,53] Furthermore, the SPPs are both launched and detected by the AFM tip, generating an interference pattern, as the waves are scattered or reflected at graphene edges, grain boundaries, or defects.[52−54] Thus, the SNOM images provide details on the spatially resolved electronic structure, as it is influenced by, for example, doping or strain. Here, such images are expected to provide insights as to how the optoelectronic properties of graphene might be spatially modulated by the pore structures. The templated SAMs can alter both the dielectric constant of the substrate[55−58] and the intrinsic substrate-induced doping of graphene on SiO_2,[15] while covalently binding graphene to PFPA can further impact the influence of charge puddles or electronic defects that serve as additional reflectors of the propagating SPP in the graphene flake.

Figure 8 shows representative 1 μm × 1 μm images of the topographic and corresponding s-SNOM images (the amplitude of the NF signal) for empty and PFPA-filled 0.5 μm pores. The SPP turnaround can be seen parallel to the graphene edges. While the scattering signal is weak, faint features such the constructive interference at the graphene edges and grain boundary patterns are still visible.

Focusing on the NF signal of the reacted graphene/PFPA pores (Figure 8B, right), four bright features corresponding to where graphene is locally bound to the PFPA pores are visible. This increase in scattering over the nanopores (notably absent in the graphene/empty pore system, Figure 8B, left) suggests that there is a localized increase in carrier density.[53] This is consistent with the DFT studies by Suggs et al. and Plachinda et al. that while the linearity of the Dirac cones is largely preserved upon reaction with the PFPA, the rehybridization of the orbitals results in an increase in the charge density where PFPA reacts; thus, causing a gap to open between the π and π^* bands of graphene.[25,26] Importantly, these results show that we can spatially alter the graphene plasmon using these simple patterning approaches, which could have significant implications in the creation of nanoscale device architectures that take advantage of simple patterning approaches to effect these optical changes.

CONCLUSIONS

Here, we have demonstrated a facile method for fabricating controlled graphene−SAM architectures using colloidal lithography to create patterned SAMs with an OTS background, onto which single-layer graphene can be deposited,

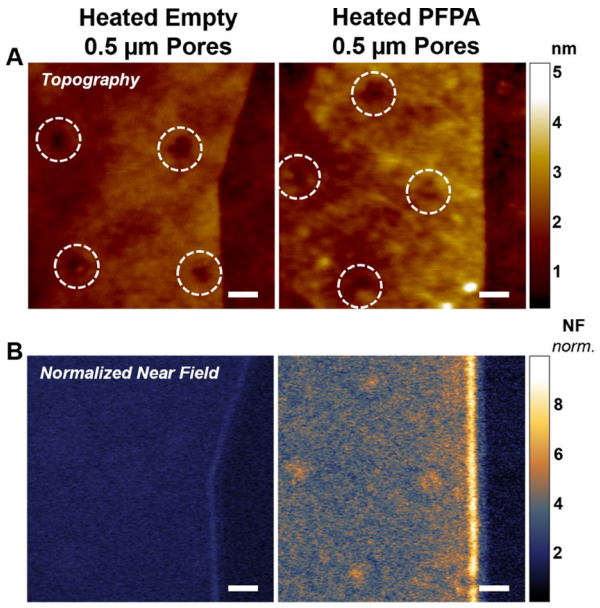

Figure 8. AFM tapping mode topography images (A) of representative areas for graphene over 0.5 μm templated empty (left) and PFPA-filled (right) pores after heating at 140 °C for 40 min. Corresponding normalized NF amplitude images (with a 10.5 μm CO_2 laser source) (B) of representative areas for graphene over 0.5 μm templated empty (left) and PFPA-filled (right) pores after heating at 140 °C for 40 min. The corresponding NF amplitude images are normalized to the amplitude signal of the bare OTS in each image. All scale bars are 0.2 μm. Pore locations are indicated with white dashed circles in the topography images.

altering its structural and optoelectronic properties. After the microsphere template was removed, the remaining periodic, hexagonally packed array of pores in OTS was then back-filled with either a chemically inert methyl-terminated SAM (C10) or a PFPA SAM known to bind to graphene upon heating. These mixed SAM-graphene architectures were characterized using AFM, ATR−FTIR, XPS, Raman microspectroscopy, and s-SNOM. The reaction of graphene with PFPA not only inhibits the out-of-plane deformation of the graphene lattice, thereby reducing the observed friction, but also alters the π conjugation of graphene resulting in the opening of a band gap,[25,26] which can in turn impact the plasmon scattering in the supported graphene on these surfaces. Overall, the ability to create such patterned architectures affords the means for investigating a myriad of mechanical, electrical, and optical properties of graphene by simple tuning of substrate interactions, making this a viable platform for screening such effects.

ASSOCIATED CONTENT

Supporting Information

The Supporting Information is available free of charge at https://pubs.acs.org/doi/10.1021/acs.langmuir.1c01136.

Histograms of the nanopore feature sizes for the various sample preparations, description of the analysis method used for the size determinations, and AFM topographic and friction images of the PFPA monolayers with graphene on silica before and after heating (PDF)

https://doi.org/10.1021/acs.langmuir.1c01136
Langmuir 2021, 37, 9996−10005

AUTHOR INFORMATION

Corresponding Author

James D. Batteas − *Department of Chemistry and Department of Materials Science and Engineering, Texas A&M University, College Station, Texas 77843, United States;* orcid.org/0000-0002-6244-5000; Email: batteas@chem.tamu.edu

Authors

Maelani Negrito − *Department of Chemistry, Texas A&M University, College Station, Texas 77843, United States*

Meagan B. Elinski − *Department of Chemistry, Texas A&M University, College Station, Texas 77843, United States;* Present Address: Department of Chemistry, Hope College, Holland, MI 49423

Nathaniel Hawthorne − *Department of Chemistry, Texas A&M University, College Station, Texas 77843, United States*

Mckenzie P. Pedley − *Department of Chemistry, Texas A&M University, College Station, Texas 77843, United States*

Mengwei Han − *Department of Civil and Environmental Engineering, University of Illinois Urbana-Champaign, Urbana, Illinois 61801, United States*

Matthew Sheldon − *Department of Chemistry and Department of Materials Science and Engineering, Texas A&M University, College Station, Texas 77843, United States*

Rosa M. Espinosa-Marzal − *Department of Civil and Environmental Engineering, University of Illinois Urbana-Champaign, Urbana, Illinois 61801, United States; Department of Materials Science and Engineering, University of Illinois Urbana-Champaign, Urbana, Illinois 61801, United States;* orcid.org/0000-0003-3442-2511

Complete contact information is available at: https://pubs.acs.org/10.1021/acs.langmuir.1c01136

Notes

The authors declare no competing financial interest.

ACKNOWLEDGMENTS

We gratefully acknowledge financial support from the National Science Foundation under grants DMR-1904887 to J.D.B. and DMR-1904681 to R.E.M. J.D.B. also acknowledges support from the Texas A&M University President's Excellence Fund X-Grants Program (project ID #291). The reaction studies of PFPA with graphene were partially supported under the NSF Center for the Mechanical Control of Chemistry (CHE-2023644).

REFERENCES

(1) Berman, D.; Deshmukh, S. A.; Sankaranarayanan, S. K. R. S.; Erdemir, A.; Sumant, A. V. Extraordinary Macroscale Wear Resistance of One Atom Thick Graphene Layer. *Adv. Funct. Mat.* **2014**, *24*, 6640−6646.

(2) Berman, D.; Deshmukh, S. A.; Sankaranarayanan, S. K. R. S.; Erdemir, A.; Sumant, A. V. Macroscale Superlubricity Enabled by Graphene Nanoscroll Formation. *Science* **2015**, *348*, 1118−1122.

(3) Novoselov, K. S.; Geim, A. K.; Morozov, S. V.; Jiang, D.; Zhang, Y.; Dubonos, S. V.; Grigorieva, I. V.; Firsov, A. A. Electric Field Effect in Atomically Thin Carbon Films. *Science* **2004**, *306*, 666−669.

(4) Peng, Y.; Wang, Z.; Zou, K. Friction and Wear Properties of Different Types of Graphene Nanosheets as Effective Solid Lubricants. *Langmuir* **2015**, *31*, 7782−7791.

(5) Liu, L.; Zhou, M.; Jin, L.; Li, L.; Mo, Y.; Su, G.; Li, X.; Zhu, H.; Tian, Y. Recent Advances in Friction and Lubrication of Graphene and Other 2D Materials: Mechanisms and Applications. *Friction* **2019**, *7*, 199−216.

(6) Mandelli, D.; Leven, I.; Hod, O.; Urbakh, M. Sliding Friction of Graphene/Hexagonal -Boron Nitride Heterojunctions: a Route to Robust Superlubricity. *Sci. Rep.* **2017**, *7*, 10851.

(7) Sinclair, R. C.; Suter, J. L.; Coveney, P. V. Graphene-Graphene Interactions: Friction, Superlubricity, and Exfoliation. *Adv. Mater.* **2018**, *30*, No. e1705791.

(8) Spear, J. C.; Custer, J. P.; Batteas, J. D. The Influence of Nanoscale Roughness and Substrate Chemistry on the Frictional Properties of Single and Few Layer Graphene. *Nanoscale* **2015**, *7*, 10021−10029.

(9) Zeng, X.; Peng, Y.; Lang, H. A Novel Approach to Decrease Friction of Graphene. *Carbon* **2017**, *118*, 233−240.

(10) Peng, Y.; Zeng, X.; Liu, L.; Cao, X.; Zou, K.; Chen, R. Nanotribological Characterization of Graphene on Soft Elastic Substrate. *Carbon* **2017**, *124*, 541−546.

(11) Lee, C.; Li, Q.; Kalb, W.; Liu, X. Z.; Berger, H.; Carpick, R. W.; Hone, J. Frictional Characteristics of Atomically Thin Sheets. *Science* **2010**, *328*, 76−80.

(12) Cho, D.-H.; Wang, L.; Kim, J.-S.; Lee, G.-H.; Kim, E. S.; Lee, S.; Lee, S. Y.; Hone, J.; Lee, C. Effect of Surface Morphology on Friction of Graphene on Various Substrates. *Nanoscale* **2013**, *5*, 3063−3069.

(13) Elinski, M. B.; Menard, B. D.; Liu, Z.; Batteas, J. D. Adhesion and Friction at Graphene/Self-Assembled Monolayer Interfaces Investigated by Atomic Force Microscopy. *J. Phys. Chem. C* **2017**, *121*, 5635−5641.

(14) Sreeprasad, T. S.; Berry, V. How Do the Electrical Properties of Graphene Change with its Functionalization? *Small* **2013**, *9*, 341−350.

(15) Wang, Q. H.; Jin, Z.; Kim, K. K.; Hilmer, A. J.; Paulus, G. L. C.; Shih, C.-J.; Ham, M.-H.; Sanchez-Yamagishi, J. D.; Watanabe, K.; Taniguchi, T.; Kong, J.; Jarillo-Herrero, P.; Strano, M. S. Understanding and Controlling the Substrate Effect on Graphene Electron-Transfer Chemistry via Reactivity Imprint Lithography. *Nat. Chem.* **2012**, *4*, 724−732.

(16) Baltazar, J.; Sojoudi, H.; Paniagua, S. A.; Kowalik, J.; Marder, S. R.; Tolbert, L. M.; Graham, S.; Henderson, C. L. Facile Formation of Graphene P−N Junctions Using Self-Assembled Monolayers. *J. Phys. Chem. C* **2012**, *116*, 19095−19103.

(17) Hwang, E. H.; Adam, S.; Sarma, S. D. Carrier Transport in Two-Dimensional Graphene Layers. *Phys. Rev. Lett.* **2007**, *98*, 186806.

(18) Liu, L.-H.; Yan, M. Functionalization of Pristine Graphene with Perfluorophenyl Azides. *J. Mater. Chem.* **2011**, *21*, 3273.

(19) Balog, R.; Jørgensen, B.; Nilsson, L.; Andersen, M.; Rienks, E.; Bianchi, M.; Fanetti, M.; Lægsgaard, E.; Baraldi, A.; Lizzit, S.; Sljivancanin, Z.; Besenbacher, F.; Hammer, B.; Pedersen, T. G.; Hofmann, P.; Hornekær, L. Bandgap Opening in Graphene Induced by Patterned Hydrogen Adsorption. *Nat. Mater.* **2010**, *9*, 315−319.

(20) Dvorak, M.; Oswald, W.; Wu, Z. Bandgap Opening by Patterning Graphene. *Sci. Rep.* **2013**, *3*, 2289.

(21) Pedersen, T. G.; Flindt, C.; Pedersen, J.; Mortensen, N. A.; Jauho, A.-P.; Pedersen, K. Graphene Antidot Lattices: Designed Defects and Spin Qubits. *Phys. Rev. Lett.* **2008**, *100*, 136804.

(22) Son, Y.-W.; Cohen, M. L.; Louie, S. G. Energy Gaps in Graphene Nanoribbons. *Phys. Rev. Lett.* **2006**, *97*, 216803.

(23) Brownfield, A. L.; Causey, C. P.; Mullen, T. J. Influence of Solvent on Octadecyltrichlorosilane Nanostructures Fabricated Using Particle Lithography. *J. Phys. Chem. C* **2015**, *119*, 12455−12463.

(24) Liu, L.-H.; Zorn, G.; Castner, D. G.; Solanki, R.; Lerner, M. M.; Yan, M. A Simple and Scalable Route to Wafer-Size Patterned Graphene. *J. Mater. Chem.* **2010**, *20*, 5041−5046.

(25) Suggs, K.; Reuven, D.; Wang, X.-Q. Electronic Properties of Cycloaddition-Functionalized Graphene. *J. Phys. Chem. C* **2011**, *115*, 3313−3317.

(26) Plachinda, P.; Evans, D.; Solanki, R. Electrical Conductivity of PFPA Functionalized Graphene. *Solid State Electron.* **2013**, *79*, 262−267.
(27) Park, J.; Yang, X.; Wickramasinghe, D.; Sundhoro, M.; Orbey, N.; Chow, K.-F.; Yan, M. Functionalization of Pristine Graphene for the Synthesis of Covalent Graphene−Polyaniline Nanocomposite. *RSC Adv.* **2020**, *10*, 26486−26493.
(28) Song, J.; Kam, F.-Y.; Png, R.-Q.; Seah, W.-L.; Zhuo, J.-M.; Lim, G.-K.; Ho, P. K. H.; Chua, L.-L. A General Method for Transferring Graphene onto Soft Surfaces. *Nat. Nanotechnol.* **2013**, *8*, 356−362.
(29) Ferrari, A. C.; Meyer, J. C.; Scardaci, V.; Casiraghi, C.; Lazzeri, M.; Mauri, F.; Piscanec, S.; Jiang, D.; Novoselov, K. S.; Roth, S.; Geim, A. K. Raman Spectrum of Graphene and Graphene Layers. *Phys. Rev. Lett.* **2006**, *97*, 187401.
(30) Ferrari, A. C.; Basko, D. M. Raman Spectroscopy as a Versatile Tool for Studying the Properties of Graphene. *Nat. Nanotechnol.* **2013**, *8*, 235−246.
(31) Lee, J. E.; Ahn, G.; Shim, J.; Lee, Y. S.; Ryu, S. Optical Separation of Mechanical Strain from Charge Doping in Graphene. *Nat. Commun.* **2012**, *3*, 1024.
(32) Lee, T.; Mas'ud, F. A.; Kim, M. J.; Rho, H. Spatially Resolved Raman Spectroscopy of Defects, Strains, and Strain Fluctuations in Domain Structures of Monolayer Graphene. *Sci. Rep.* **2017**, *7*, 16681.
(33) Liu, C.; Ma, Y.; Li, W.; Dai, L. The Evolution of Raman Spectrum of Graphene with the Thickness of SiO2 Capping Layer on Si Substrate. *Appl. Phys. Lett.* **2013**, *103*, 213103.
(34) Martins Ferreira, E. H.; Moutinho, M. V. O.; Stavale, F.; Lucchese, M. M.; Capaz, R. B.; Achete, C. A.; Jorio, A. Evolution of the Raman Spectra from Single-, Few-, and Many-lLayer Graphene with Increasing Disorder. *Phys. Rev. B: Condens. Matter Mater. Phys.* **2010**, *82*, 125429.
(35) Yoon, D.; Son, Y.-W.; Cheong, H. Negative Thermal Expansion Coefficient of Graphene Measured by Raman Spectroscopy. *Nano Lett.* **2011**, *11*, 3227−3231.
(36) Zorn, G.; Liu, L.-H.; Árnadóttir, L.; Wang, H.; Gamble, L. J.; Castner, D. G.; Yan, M. X-Ray Photoelectron Spectroscopy Investigation of the Nitrogen Species in Photoactive Perfluorophenylazide-Modified Surfaces. *J. Phys. Chem. C* **2014**, *118*, 376−383.
(37) Sader, J. E.; Chon, J. W. M.; Mulvaney, P. Calibration of Rectangular Atomic Force Microscope Cantilevers. *Rev. Sci. Instrum.* **1999**, *70*, 3967−3969.
(38) Barad, H.-N.; Kwon, H.; Alarcón-Correa, M.; Fischer, P. Large Area Patterning of Nanoparticles and Nanostructures: Current Status and Future Prospects. *ACS Nano* **2021**, *15*, 5861−5875.
(39) Barriga, J.; Coto, B.; Fernandez, B. Molecular Dynamics Study of Optimal Packing Structure of OTS Self-Assembled Monolayers on SiO2 Surfaces. *Tribol. Int.* **2007**, *40*, 960−966.
(40) Peters, R. D.; Nealey, P. F.; Crain, J. N.; Himpsel, F. J. A Near Edge X-ray Absorption Fine Structure Spectroscopy Investigation of the Structure of Self-Assembled Films of Octadecyltrichlorosilane. *Langmuir* **2002**, *18*, 1250−1256.
(41) Tillman, N.; Ulman, A.; Schildkraut, J. S.; Penner, T. L. Incorporation of Phenoxy Groups in Self-Assembled Monolayers of Trichlorosilane Derivatives: Effects on Film Thickness, Wettability, and Molecular Orientation. *J. Am. Chem. Soc.* **1988**, *110*, 6136−6144.
(42) Wasserman, S. R.; Whitesides, G. M.; Tidswell, I. M.; Ocko, B. M.; Pershan, P. S.; Axe, J. D. The Structure of Self-Assembled Monolayers of Alkylsiloxanes on Silicon: A Comparison of Results from Ellipsometry and Low-Angle X-ray Reflectivity. *J. Am. Chem. Soc.* **1989**, *111*, 5852−5861.
(43) Wang, X.; Tantiwanichapan, K.; Christopher, J. W.; Paiella, R.; Swan, A. K. Uniaxial Strain Redistribution in Corrugated Graphene: Clamping, Sliding, Friction, and 2D Band Splitting. *Nano Lett.* **2015**, *15*, 5969−5975.
(44) Bao, W.; Miao, F.; Chen, Z.; Zhang, H.; Jang, W.; Dames, C.; Lau, C. N. Controlled Ripple Texturing of Suspended Graphene and Ultrathin Graphite Membranes. *Nat. Nanotechnol.* **2009**, *4*, 562−566.
(45) Larsen, M. B. B. S.; Mackenzie, D. M. A.; Caridad, J. M.; Bøggild, P.; Booth, T. J. Transfer Induced Compressive Strain in Graphene: Evidence from Raman Spectroscopic Mapping. *Microelectron. Eng.* **2014**, *121*, 113−117.
(46) Zhang, S. H.; Hou, Y.; Li, S.; Zhang, Z.; Feng, X.-Q.; Li, Q. Tuning Friction to a Superlubric State via In-Plane Straining. *Proc. Natl. Acad. Sci. U.S.A.* **2019**, *116*, 24452−24456.
(47) Kitt, A. L.; Qi, Z.; Rémi, S.; Park, H. S.; Swan, A. K.; Goldberg, B. B. How Graphene Slides: Measurement and Theory of Strain-Dependent Frictional Forces Between Graphene and SiO2. *Nano Lett.* **2013**, *13*, 2605−2610.
(48) Saito, R.; Jorio, A.; Souza Filho, A. G.; Dresselhaus, G.; Dresselhaus, M. S.; Pimenta, M. A. Probing Phonon Dispersion Relations of Graphite by Double Resonance Raman Scattering. *Phys. Rev. Lett.* **2002**, *88*, 027401.
(49) Cançado, L. G.; Jorio, A.; Pimenta, M. A. Measuring the Absolute Raman Cross Section of Nanographites as a Function of Laser Energy and Crystallite Size. *Phys. Rev. B: Condens. Matter Mater. Phys.* **2007**, *76*, 064304.
(50) Tian, S.; Yang, Y.; Liu, Z.; Wang, C.; Pan, R.; Gu, C.; Li, J. Temperature-Dependent Raman Investigation on Suspended Graphene: Contribution from Thermal Expansion Coefficient Mismatch Between Graphene and Substrate. *Carbon* **2016**, *104*, 27−32.
(51) Tripathi, M.; Lee, F.; Michail, A.; Anestopoulos, D.; McHugh, J. G.; Ogilvie, S. P.; Large, M. J.; Graf, A. A.; Lynch, P. J.; Parthenios, J.; Papagelis, K.; Roy, S.; Saadi, M. A. S. R.; Rahman, M. M.; Pugno, N. M.; King, A. A. K.; Ajayan, P. M.; Dalton, A. B. Structural Defects Modulate Electronic and Nanomechanical Properties of 2D Materials. *ACS Nano* **2021**, *15*, 2520−2531.
(52) Chen, J.; Badioli, M.; Alonso-González, P.; Thongrattanasiri, S.; Huth, F.; Osmond, J.; Spasenović, M.; Centeno, A.; Pesquera, A.; Godignon, P.; Zurutuza Elorza, A.; Camara, N.; de Abajo, F. J. G.; Hillenbrand, R.; Koppens, F. H. L. Optical Nano-Imaging of Gate-Tunable Graphene Plasmons. *Nature* **2012**, *487*, 77−81.
(53) Fei, Z.; Rodin, A. S.; Andreev, G. O.; Bao, W.; McLeod, A. S.; Wagner, M.; Zhang, L. M.; Zhao, Z.; Thiemens, M.; Dominguez, G.; Fogler, M. M.; Neto, A. H. C.; Lau, C. N.; Keilmann, F.; Basov, D. N. Gate-Tuning of Graphene Plasmons Revealed by Infrared Nano-Imaging. *Nature* **2012**, *487*, 82−85.
(54) Gerber, J. A.; Berweger, S.; O'Callahan, B. T.; Raschke, M. B. Phase-Resolved Surface Plasmon Interferometry of Graphene. *Phys. Rev. Lett.* **2014**, *113*, 055502.
(55) Campbell, I. H.; Kress, J. D.; Martin, R. L.; Smith, D. L.; Barashkov, N. N.; Ferraris, J. P. Controlling Charge Injection in Organic Electronic Devices Using Self-Assembled Monolayers. *Appl. Phys. Lett.* **1997**, *71*, 3528−3530.
(56) Israelachvili, J. N. *Intermolecular and Surface Forces*, 3 ed.; Elsevier Inc.: 30 Corporate Drive, Suite 400, Burlington, MA 01803, USA, 2011; p 710.
(57) Kobayashi, S.; Nishikawa, T.; Takenobu, T.; Mori, S.; Shimoda, T.; Mitani, T.; Shimotani, H.; Yoshimoto, N.; Ogawa, S.; Iwasa, Y. Control of Carrier Density by Self-Assembled Monolayers in Organic Field-Effect Transistors. *Nat. Mater.* **2004**, *3*, 317−322.
(58) Yan, Z.; Sun, Z.; Lu, W.; Yao, J.; Zhu, Y.; Tour, J. M. Controlled Modulation of Electronic Properties of Graphene by Self-Assembled Monolayers on SiO2 Substrates. *ACS Nano* **2011**, *5*, 1535−1540.

https://doi.org/10.1021/acs.langmuir.1c01136
Langmuir 2021, 37, 9996−10005